Chapter 0

Fourier transform spectroscopy with partially scanned interferograms as a tool to retrieve atmospheric gases concentrations from high spectral resolution satellite observations. Methodological aspects and application to IASI.

Carmine Serio, Guido Masiello

CNISM, Unitá di Ricerca di Potenza, Universitá della Basilicata, 85100 Potenza

Italy

Giuseppe Grieco

DIFA, Universitá della Basilicata, 85100 Potenza

Italy

1. Introduction

Fourier Transform Spectroscopy with partially scanned interferograms (FTS*PSI) is a technique to obtain the difference between spectra of atmospheric radiance at two diverse spectral resolutions (Grieco et al., 2010; 2011; Kyle, 1977; Smith et al., 1979).

In the context of infrared remote sensing, the idea of using partially scanned interferograms for the retrieval of atmospheric parameters dates back to Kyle (1977) who argued that large portions of the spectrum (the Fourier transform of the interferogram and vice versa) could bring poor or no information for a given atmospheric parameter, whereas small ranges in the interferogram domain could concentrate much information about the parameter at hand. Kyle (1977) exemplified the techniques for temperature, whereas a correlation interferometer was proposed for the observation of atmospheric trace gases by Goldstein et al. (1978). The direct inversion of small segments of interferometric radiances for the purpose of temperature retrieval was further analyzed and exemplified in Smith et al. (1979).

In some circumstances, according to Kyle (1977) the interferogram domain can provide a data space in which information about the atmospheric thermodynamical state can be encoded much more efficiently than in the spectral domain. Exploiting this idea, Grieco et al. (2010) has shown how to perform a dimensionality reduction of high spectral resolution infrared observations, which preserves the spectral coverage of the original spectrum . Once compared to the usual way of reducing a high amount of spectral data by simply considering a sparse (optimal) selection of the spectral channels, the methodology has shown a better performance mostly for the retrieval of water vapor.

Unlike the previous works by Grieco et al. (2010); Kyle (1977); Smith et al. (1979), which concentrated on the direct use of inteferogram radiances, in this study, we consider the point of transforming back to the spectral domain the partial scanned interferogram, in such a way to obtain a difference spectrum with improved signal-to-noise ratio. This difference spectrum, instead of the partial interferogram, is considered for the retrieval of atmospheric gases. Depending on the interferogram range, the difference spectrum can isolate emission features of atmospheric gases from, e.g., the strong surface emission. In this respect the technique is mostly suited for nadir looking radiometers/spectrometers on board of satellites, since for this instrumentation the observed infrared radiance is made up by the atmospheric component plus that of surface emission. The issue of properly choosing the partial interferogram has to do with correlation interferometry. Because of the Wiener-Khinchin-Einstein theorem (e.g. see Bell (1972)), the interferogram is the *auto*-correlation function of the light spectrum, which means that periodic or almost periodic features present in the spectrum can yield sharp peaks (constructive interference). in the interferogram signal. As an example for the specific case of CO_2, rotation transitions yield a spectrum characterized by a periodic pattern with a period of about 1.5 cm^{-1}. This periodic pattern determines a strong signature (coherent interference) in the interferogram domain at about 1/1.5 cm=0.66 cm and overtones. Thus, for the case of CO_2, molecular spectroscopy fundamentals tell us how to exactly choose the proper partial interferogram.

In this study, FTS*PSI will be exemplified to show how we can handle and partly separate from the spectrum the surface emission in order to develop and implement suitable schemes for the retrieval of the columnar load of CO_2, CO, CH_4 and N_2O. The methodology will be applied to the Infrared Atmospheric Sounding Interferometer (IASI), which is flying on board the Metop-A (Meteorological Operational Satellite) platform. IASI was developed in France by the Centre National d'Etudes Spatiales (CNES) and is the first of three satellites of the European Organization for the Exploitation of Meteorological Satellite (EUMETSAT) European Polar System (EPS). The instrument spectral bandwidth covers the range from 645 to 2760 cm^{-1} (3.62 to 15.50 μm), with a sampling interval $\Delta\sigma = 0.25$ cm^{-1}. Thus, each single spectrum yields 8461 data points or channels. The calibrated IASI interferogram extends from 0 to a maximum OPD of 2 cm.

As already outlined, the main objective of this study is to illustrate, demonstrate and exemplify the potential advantages of high infrared spectral resolution observations data analysis with partially scanned interferograms, through the exploitation of IASI data. Towards this objective, we have used a forward/inverse methodology to which we refer to as φ-IASI, whose mathematical aspects and validation has been largely documented (see e.g. Amato et al. (2002); Carissimo et al. (2005); Grieco et al. (2007); Masiello et al. (2002; 2003; 2004); Masiello & Serio (2004); Masiello et al. (2009; 2011); Serio et al. (2000)).

The remote sensing of atmospheric minor and trace gases from nadir looking instrumentation on board polar satellites is not a new subject. Among many others we quote here the experience with the Japanese IMG (Interferometric Monitoring of Greenhouse Gases) (Lubrano et al., 2004), the American AIRS (Atmospheric Infrared Radiometer Sounder) (Chahine et al, 2005; 2008; McMillan et al., 2005) and the European IASI (Boynard et al., 2009; Clarisse et al., 2008; 2009; Clerbaux et al., 2009; Crevoisier et al., 2009; Grieco et al., 2011; Ricaud et al., 2009). However, this work is focused mostly on the novel methodology of FTS*PSI rather than particular applications, which nevertheless are here considered to exemplify the use of the procedure for the remote sensing of minor and trace gases.

The study is organized as follows. Section 2 is mainly devoted to the methodological aspects: in section 2.1 we present the IASI data, whereas the description of the fundamentals of the partially scanned interferogram approach is presented in sections 2.2, 2.2.1 and 2.3. Application to IASI for the retrieval of CO_2, CO, CH_4 and N_2O is discussed in sections 3, 4, 5 and 6, respectively. Section 3, which covers the case of CO_2 is mainly intended to exemplify the overall methodology. Results for CO_2 concerning the quality and validation of the methodology have been recently presented in Grieco et al. (2011). These results will not be shown here again, but only summarized for the benefit of the reader in section 3.3. However, the material shown in the two methodological sections, 3.1, and 3.2 is largely complementary to that presented in Grieco et al. (2011) and address important aspects, which generalize the application of the methodology to the full disk. Conversely, the results for CO, CH_4 and N_2O, shown in sections 4, 5 and 6, are presented here for the first time and have not been covered in previous publications by the authors. Conclusions are drawn in section 7.

2. Background

2.1 IASI data

For the purpose of simulations we use the Chevalier data set (Chevalier, 2001). This set is mostly used to define pairs of IASI spectra and atmospheric state vectors.

Real IASI observations and related atmospheric state vectors come from the 2007 Joint Airborne IASI Validation Experiment (JAIVEx) campaign JAIVEx (2007) over the Gulf of Mexico. We have a series of 6 spectra for 29 April 2007, 16 spectra for 30 April 2007, and finally 3 spectra for 04 May 2007. The spectra where recorded for clear sky fields of view, selected based on high resolution satellite imagery from AVHRR (Advanced Very High Resolution Radiometer) on MetOp (Meteorological Operational Satellite) and in-flight observations. Furthermore, the data for 29 April 2007 correspond to a nadir IASI field view, whereas those for the other two days to a field of view of 22.50 degrees.

Dropsonde and ECMWF (European Centre for Medium range Weather Forecasts) model data, which have been used to have a best estimate of the atmospheric state during each MetOp overpass, have been prepared and made available to us by the JAIVEx team. The JAIVEx dataset contains dropsonde profiles of temperature, water vapor, ozone, and carbon monoxide which extend up to 400 hPa. Above 400 hPa only ECMWF model data are available. The atmospheric state vectors used in this study use JAIVex dropsonde data up to 400 hPa supplemented by collocated ECMWF forecasts of temperature, water vapor and ozone from 400 hPa to 0.1 hPa (corresponding to about 65 km).

For the purpose of atmospheric gas retrieval we have also used IASI data for a monthly acquisition on July 2010 over the Mediterranean area. These data set has been used to produce monthly maps for the four gases at hand. The spectra were checked for clear sky using the IASI stand alone cloud detection scheme developed by Grieco et al. (2007); Masiello et al. (2002; 2003; 2004); Serio et al. (2000).

2.2 Basic aspects of FTS⋆PSI

The principles of FTS⋆PSI have been recently discussed in Grieco et al. (2011), here we limit to show the basic aspects. FTS⋆PSI is a particular application of Fourier spectroscopy, which today counts widespread applications in many fields. Fourier spectroscopy fundamentals can be found in appropriate textbooks (see e.g. Bell (1972)). A summary of the basic definitions, which are relevant to our methodology is now presented.

In Fourier spectroscopy the spectrum, $r(\sigma)$ (with σ the wavenumber) and the interferogram, $I(x)$ (with x the optical path difference) constitute a Fourier pair defined by the couple of equations (see e.g. Bell (1972)),

$$r(\sigma) = \int_{-\infty}^{+\infty} I(x) \exp(-2\pi i \sigma x) dx \tag{1}$$

$$I(x) = \int_{-\infty}^{+\infty} r(\sigma) \exp(2\pi i \sigma x) d\sigma \tag{2}$$

with i the imaginary unit. The spectrum and the interferogram are in practice band-limited functions, therefore taking into account that the interferogram is sampled up to a given maximum optical path difference, x_{max}, we modify Eq. (1) by introducing the data-sampling window, $W(x)$

$$r(\sigma) = \int_{-\infty}^{+\infty} W(x) I(x) \exp(-2\pi i \sigma x) dx \tag{3}$$

with

$$W(x) = \begin{cases} 1 \text{ for } \mid x \mid \leq x_{max} \\ 0 \quad \text{otherwise} \end{cases} \tag{4}$$

where $\mid \cdot \mid$ means absolute value, x_{max} is the maximum optical path difference.

The maximum optical path difference, x_{max} also determines the sampling rate, $\Delta\sigma$ within the spectral domain. According to the Nyquist rule, the relation is

$$\Delta\sigma = \frac{1}{2x_{max}}, \quad \Delta x = \frac{1}{2(\sigma_2 - \sigma_1)} \tag{5}$$

where $\sigma_2 - \sigma_1$ is the spectral band-width. For IASI we have $\sigma_1 = 645$ cm^{-1}, $\sigma_2 = 2760$ cm^{-1}, hence $x_{max} = 2$ cm and $\Delta\sigma = 0.25$ cm^{-1}.

The fact that IASI is apodized (see e.g. Amato et al. (1998)) is of no concern here. For IASI we just consider the interferogram obtained from the calibrated, apodized spectrum. One could also consider to obtain the interferogram corresponding to each IASI band one at a time. This is appropriate, e.g., when dealing with a given gas whose absorption bands are confined within a single IASI band.

According to the Shannon-Whittaker sampling theorem (e.g. see (Robinson & Silvia, 1981)), in case we want to re-sample the spectrum at a sampling rate lower than the original, we just have to introduce in Eq. (3) a data-sampling window with its new cutting point at $x_\tau < x_{max}$. The new sampling rate, $\Delta\sigma_\tau$ appropriate to x_τ involves again the Nyquist rule, we have $\Delta\sigma_\tau = (2x_\tau)^{-1}$.

2.2.1 The couple partial interferogram, difference spectrum

For a nadir viewing instrument such as IASI, one of the most prominent feature within the observations is the surface emission. This emission allows us to retrieve skin temperature and have information about surface emissivity. However, in case we are interested in retrieving atmospheric parameters, such as minor gases, we would like to have information only about atmospheric emission, since the surface emission interferes with the signal we want to exploit for the retrieval process.

As opposite to gas emission, surface emission varies smoothly with the wave number, σ. Thus, if we consider two spectral samplings, $\Delta\sigma_1$, $\Delta\sigma_2$, which are close each other but small enough so that the surface emission has been resolved at either samplings, then the difference spectrum

$$d(\sigma) = r_1(\sigma) - r_2(\sigma) \tag{6}$$

contains mostly the atmospheric emission alone. In Eq. 6, r_i is the spectrum at sampling $\Delta\sigma_i$, with $i = 1, 2$.

In reality, the above differentiation cannot get completely rid of the surface emission, because the surface emission term of the Top of the Atmosphere (TOA) spectrum is modulated by the total transmittance function, which is itself a highly oscillatory function. However, in window regions where the transmittance approximates the unity, and where gases have only weak absorption bands, the difference $d(\sigma)$ yields a signal, which is mostly the result of atmospheric emission alone.

It is important here to stress that to compute the difference spectrum, $d(\sigma)$ we do not need to measure the spectrum twice. The operation can be done by simply Fourier transforming one single *partial* interferogram. In fact, with reference to Eq. 6 and provided that, $\Delta\sigma_i > \Delta\sigma$ ($i = 1, 2$), and with $\Delta\sigma$ defined by Eq. 5, that is the sampling rate corresponding to the maximum optical path difference, we have that $d(\sigma)$ corresponds to the interferogram, $I(x)$ computed over the range $[x_1, x_2]$, with

$$x_1 = (2\Delta\sigma_2)^{-1}; \quad x_2 = (2\Delta\sigma_1)^{-1} \tag{7}$$

where, to fix the idea we have assumed $\Delta\sigma_1 < \Delta\sigma_2$. Therefore, $d(\sigma)$ can be computed by Fourier transforming the *partial* interferogram, $I_p(x)$ defined by

$$\begin{cases} I_p(x) = 0 & \text{for} \quad x < x_1 \\ I_p(x) = I(x) & \text{for} \quad x_1 \leq x \leq x_2 \\ I_p(x) = 0 & \text{for} \quad x_2 < x \leq x_{max} \end{cases} \tag{8}$$

The left and right zero-padding ensures that the difference spectrum is defined on the same σ-grid as that corresponding to the sampling rate $\Delta\sigma$.

For the purpose of Fourier Transform computations, the above concept of partial interferogram is better formalized by considering an appropriate data-sampling window with a lower and upper truncation point (Grieco et al., 2011; Kyle, 1977),

$$\tilde{W}(x) = \begin{cases} 1 \text{ for } x_1 \leq \mid x \mid \leq x_2 \\ 0 \qquad \text{otherwise} \end{cases} \tag{9}$$

This data-sampling window removes from the spectrum all those broad features, which are represented by interferometric radiances below the left truncation point, x_1. In fact we have

$$\tilde{W}(x) = W_2(x) - W_1(x) \tag{10}$$

where W is the box-car window as defined in Eq. (4) and where the under scripts 1 and 2 identify the window function with cutting points, x_1 and x_2, respectively. Because the Fourier transform is linear, within the spectral domain, the double-truncation data-sampling window is equivalent to take the difference of Eq. 6.

An example of partial interferogram is provided in Fig. 1, where it is also exemplified that the difference spectrum enhances the atmospheric emission, while the broad surface emission is almost zeroed.

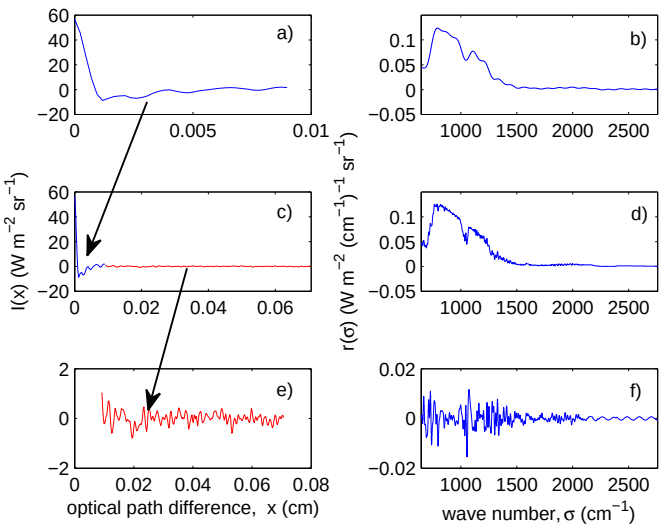

Fig. 1. Examples of couples (interferogram, spectrum) for different optical path differences. The couple a) b) refers to $x = 0.1$ cm, the couple c) d), to $x = 0.2$ cm. Couple e) f) exemplifies that the partial interferogram in the range $[0.1, 0.2]$ cm, corresponds to the difference of the spectra d)-b).

Another important characteristic of FTS⋆PSI is that the difference spectrum can be observed with enhanced signal-to-noise ratio with respect to the whole spectrum, $r(\sigma)$, that is to the spectrum corresponding to the maximum optical depth difference. According to a well-known results of Fourier spectroscopy (Pichett & Strauss, 1972), the spectral noise

variance is proportional to the interferogram bandwidth $\Delta x = x_2 - x_1$. In case we consider the full interferogram, Δx is exactly the maximum optical path difference, which for IASI is 2 cm. As a consequence, the variance of $d(\sigma)$ is simply computed in case we know the variance of $r(\sigma)$, that is the radiometric noise affecting the spectral radiances.

The radiometric noise for $r(\sigma)$ we have used in this paper is the IASI L1C radiometric noise, which is shown in Fig. 2 Let $\varepsilon(\sigma)$ be the radiometric noise affecting the spectrum, $r(\sigma)$. For

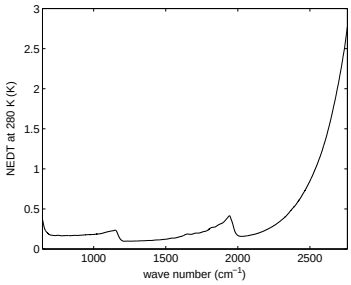

Fig. 2. IASI level 1C radiometric noise in terms of Noise Equivalent Difference Temperature (NEDT) at as scene temperature of 280 K.

the difference spectrum $d(\sigma)$, the noise is

$$\varepsilon_\Delta(\sigma) = \varepsilon(\sigma)\sqrt{\frac{x_2 - x_1}{x_{max}}} \tag{11}$$

where the underscript Δ refers to the difference spectrum.

Strictly speaking, Eq. 11 applies to the case of uncorrelated noise, that is in case the noise affecting the original spectrum, $r(\sigma)$ is truly random. However, this is not the case for IASI, because IASI data are Gaussian apodized (Amato et al., 1998). However, in section 3 we will see that, at least for IASI, Eq. 11 provides a good reference to have the order of magnitude of the noise reduction in the transformed difference-spectrum space.

However, whatever the kind of noise (correlated or uncorrelated) in the original spectrum space may be, to obtain $d(\sigma)$ we use zero padding in order not to modify the IASI sampling of 0.25 cm^{-1}. This means that the noise in the d-spectrum space is correlated.

2.3 Sensitivity of $d(\sigma)$-channels to the atmospheric state vector

When properly defined, the difference spectrum, $d(\sigma)$ is expected to be less sensitive to the atmospheric state, but the given parameter whose signal we want to amplify, than the original spectrum, $r(\sigma)$.

To quantitatively analyze this aspect we introduce an obvious measure of the sensitivity of $d(\sigma)$ to a given parameter. This measure makes use of the Jacobian derivative.

For each given channel or wavenumber, σ The noise-normalized sensitivity to a generic parameter, $\mathbf{X}$, is defined and computed according to

$$\mathbf{S}_{X,\Delta}(\sigma) = \left(\frac{1}{\varepsilon_\Delta(\sigma)}\frac{\partial d(\sigma)}{\partial \mathbf{X}}\right) \tag{12}$$

where $\varepsilon_\Delta(\sigma)$ is the radiometric noise affecting the difference spectrum, $d(\sigma)$. The above sensitivity expression says how large is the noise-normalized variation of the signal at σ to a unitary perturbation of $\mathbf{X}$. Note that in general, $\mathbf{X}$ can a be a scalar (e.g. surface temperature and emissivity, in which case the sensitivity is a scalar itself, function of the wave number, σ), or a vector (e.g., temperature profile, water vapour profile), in which case the sensitivity is a vector itself, function of the wave number.

For purpose of comparison, the above sensitivity can be also defined for the case of the original IASI spectrum, $r(\sigma)$

$$\mathbf{S}_X(\sigma) = \left(\frac{1}{\varepsilon(\sigma)} \frac{\partial r(\sigma)}{\partial \mathbf{X}} \right) \tag{13}$$

3. Application to CO_2

As said in section 1, for the case of CO_2 we have that a small range around the optical path difference at 0.66 cm is mostly dominated by CO_2 emission. The resulting CO_2 signature is clearly visible in Fig. 3, which shows a partial interferogram in the range 0.65 to 0.68 cm. Transforming back to the spectral domain the partial interferogram, we obtain the difference

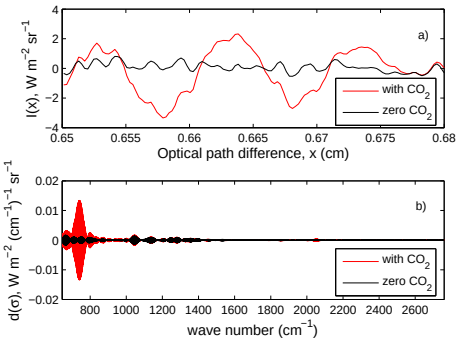

Fig. 3. a) Example of partial interferogram in the range $[x = 0.65, x = 0.68]$ cm for a case of CO_2 load equal to 0 and 385 ppmv, respectively; b) the difference spectrum $d(\sigma)$. The full IASI spectral coverage 645 to 2760 cm^{-1} has been considered.

spectrum shown in 3(b), where the CO_2-lines periodic pattern is clearly amplified.

Figure 3(b) suggests that $d(\sigma)$ is mostly a function of the CO_2 amount alone. This can be checked in simulation through generation and analysis of difference-spectra corresponding to diverse amount of CO_2.

3.1 The case of noise free radiances

We first discuss the noise-free situation. In doing so, radiative transfer calculations were performed based on the atmospheric states summarized in Fig. 4.

With reference to the tropical model of atmosphere shown in Fig. 4 (panels (a), (b) an (c)), difference spectra were generated for sixteen different columnar amounts, $q_{CO_2}(i)$, $(i =$

$1 \ldots 16$) of CO_2 ranging from 300 to 450 ppmv with a step of 10 ppmv. To perform the radiative transfer calculations, we had to assume a model of dependence on altitude for the CO_2 mixing ratio. As shown in Fig. 4, this was assumed to be constant with altitude.

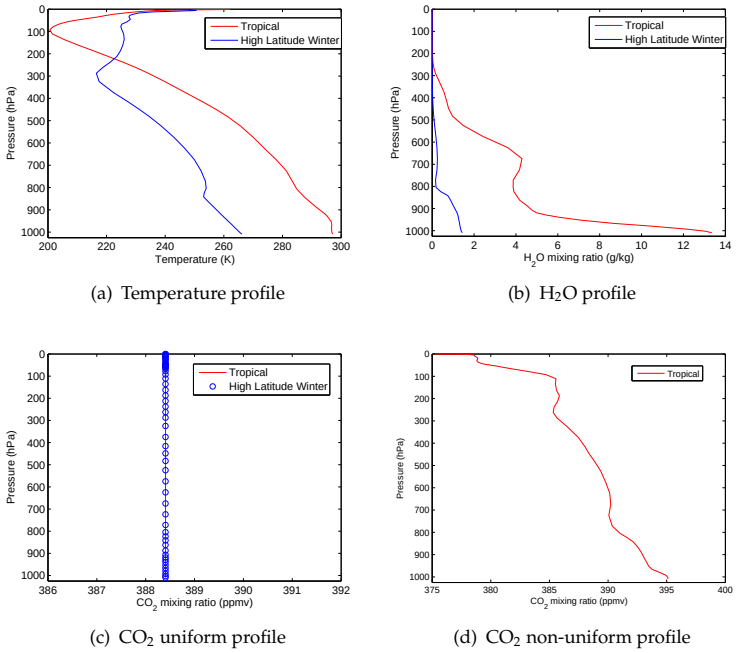

(a) Temperature profile

(b) H_2O profile

(c) CO_2 uniform profile

(d) CO_2 non-uniform profile

Fig. 4. The two reference atmosphere models used to simulate IASI synthetic radiances. The models belong to two opposite weather conditions: tropical and High Latitude Winter. As a rule, for the reference state, the CO_2 profile is assumed constant with altitude (as shown in (c)). For checking a possible dependence of the methodology on the shape of the CO_2 profile, the analysis has also considered a case of CO_2 profile non uniform with altitude (shown in (d)); this case was used in combination with the tropical model alone.

A search of the channels that are best linearly correlated with the CO_2 columnar amount shows that there are many and a few of this are largely insensitive to surface emissivity and temperature. Four of these good channels have been identified and they correspond to the wave numbers $\sigma_1 = 783.75$ cm^{-1}, $\sigma_2 = 809.25$ cm^{-1}, $\sigma_3 = 976.75$ cm^{-1}, $\sigma_4 = 2105$ cm^{-1}, respectively.

Let $d_j(i)$ be the difference spectrum ordinate corresponding to the wave number σ_j (with $j = 1 \ldots 4$) and the CO_2 columnar amount, $q_{CO_2}(i)$, (with $i = 1 \ldots 16$), respectively. For each wave number, σ_j, we consider the standardized quantity,

$$D_j(i) = \frac{d_j(i) - \mu_j}{s_j} \tag{14}$$

with μ_j and s_j the mean and standard deviation of the sample, $\{d_j(i)\}_{i=1\ldots16}$, respectively.

Figure 5(a) exemplifies, for the case of the channel at $\sigma_1 = 783.75$, that the relation between D_j and q_{CO_2} is perfectly linear, that is

$$q_{CO_2} = a_j D_j + b_j \tag{15}$$

The solid lines shown in Fig. 5 are the linear best fit to the data points. It is important to stress that the regression coefficients a_j and b_j depend on the Field of View angle. Unless otherwise stated, the results shown in this section apply to the nadir angle. In addition, it is also important to stress that even for noisy-free radiances the estimation of the column-integrated CO_2 from Eq. 15 has a residual uncertainty. This uncertainty is of the order od 1-1.5 ppmv and can be thought of as a sort of error inherited from the linearization of the dependence of q_{CO_2} on d_j. The exact amount of this uncertainty can depend on the wave number. Actually,

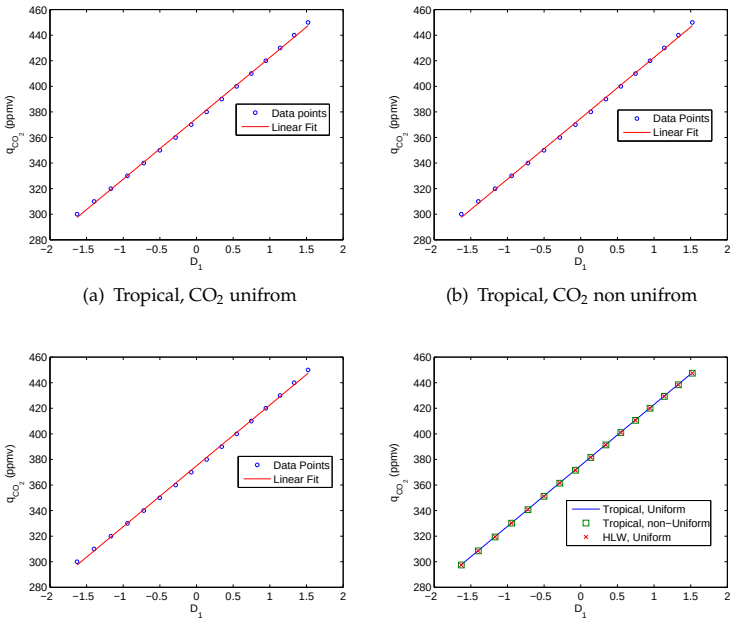

(a) Tropical, CO_2 unifrom

(b) Tropical, CO_2 non unifrom

(c) HLW, CO_2 unifrom

(d) The three linear best fits in (a), (b) and (c) are intercompared.

Fig. 5. Exemplifying the dependence of q_{CO_2} on D_j for the channel at $\sigma_1 = 783.75\ \mathrm{cm}^{-1}$ as a function of the atmosphere model (tropical and High Latitude Winter, HLW) and shape of the CO_2 profile.

the search of the *linear* channels have been done by computing the linear regression standard error at each single channel and choosing only those with standard error less than 1.5 ppmv. The typical accuracy or estimation error of q_{CO_2} estimated by Eq. 15 for the four channels at hand is shown in Tab. 1.

Table 1 (see the accuracy for the noiseless case) also shows that a linear relation holds for the remaining three channels, $\sigma_1 = 809.25\ \mathrm{cm}^{-1}$, $\sigma_3 = 976.75\ \mathrm{cm}^{-1}$, $\sigma_4 = 2105\ \mathrm{cm}^{-1}$.

Channel (cm^{-1})	Accuracy (Noise-free case) (ppmv)	Accuracy (Noisy case) (ppmv)
783.75	1.4	17.5
809.25	1.5	10.8
976.75	1.2	28.7
2105	1.1	26.2

Table 1. Accuracy of the column-integrated CO_2 amount estimated through the linear fit of Eq. 15 for the case of noise-free and noisy radiances.

More important here is the fact that the functional relation between q_{CO_2} and D_j does not depend on the assumed shape for the CO_2 profile. To check this dependence we have re-done the calculations, but now with a CO_2 mixing ratio profile, which is not constant with altitude. This altitude-varying profile (shown in Fig. 4)(d) represents a realistic situation. In fact, it is the result of the ECMWF analysis Engelen et al. (2009) corresponding to the date (29 April 2007) and location of the JAIVEx experiment. Figure 5(b) shows that the functional relation remains perfectly linear.

Moreover, the shape of the functional relation is completely independent of the state vector, as well. In fact, if we redo the calculations, but now with the High Latitude Winter model of atmosphere (see Fig. 4 from (a) to (c)), we obtain the result shown in 5c, which says that the dependence of q_{CO_2} on D_j is linear whatever the atmospheric state vector may be.

In addition, not only the linear shape does not change with the state vector and the assumed shape of the CO_2 profile, it is exactly the same (as it is shown in Fig. 5(d)). That is the regression coefficients remain constant under a varying state vector, even in the CO_2 profile shape, which means that Eq. 15 has an general or universal validity.

Once again, we stress that although Fig. 5 focuses on the channel at $\sigma_1 = 783.75$ cm^{-1}, the same results hold for all the four channels, σ_j, $j = 1, \ldots, 4$. The linearity for these channels is likely to be a results of the fact that they correspond to wing regions of strong absorption bands, or to moderate absorption bands. In general, channels inside strong absorptions bands show a behavior, which is largely non linear.

It is important to stress that while the linear dependence of q_{CO_2} on D_j is universal, this is not true for the case in which we consider the difference spectrum, d_j, since the standardization parameters, μ_j and s_j do depend on the state vector.

Since in practice we observe d_j, in case we have one single IASI spectrum, we are faced with the problem of computing μ_j and s_j to perform the standardization, which yield, D_j (see Eq. 14). The only way to go in this case is to compute a series of synthetic IASI spectra with different load of CO_2. The synthetic spectra have to be computed on the basis of the possibly best estimate of the atmospheric state vector corresponding to the given IASI observation. Thus, for *weather* applications in which we need a space-time resolved CO_2 estimation, we do need information on the atmospheric state vector.

For *climate* analysis, we need to average over many weather states. Thus, the fact that the q_{CO_2} has an universal linear dependence on D_j means that, by considering averages, we get rid of the dependence on the state vector. In practice, if we compare d_j-values properly averaged

on climate time scales, these values are directly proportional to q_{CO_2}-values averaged over the same climate time scales. As an example if we take all the IASI clear sky sea-surface tropical spectra for the year, say Y_1 and compute the mean value of d_j for whatever j (call this average $< d_{j,Y_1} >$), and redo this operation for a second year Y_2, the difference $< d_{j,Y_2} > - < d_{j,Y_1} >$ is directly proportional to the variation of the CO_2 over the time span $Y_2 - Y_1$. To accurately estimate CO_2 changes on a climate time span is an easy task from satellite observations, provided we use FTS*PSI.

3.2 Noisy radiances

With radiances affected by noise we can again just use Eq. 15 to estimates the CO_2 columnar amount. However, now the variability of the estimate is expected to increase according to the noise affecting IASI radiances.

In case of noisy radiances, taking into account Eq. 11, the accuracy can be computed through the usual rule of variance propagation. With reference to the basic Eq. 15, we have

$$\mathrm{var}\,(q_{CO_2}) = (a_j^2/s_j^2)\mathrm{var}\left(d_j\right) \tag{16}$$

where var(·) stand for variance.

Figure 6 shows the standard deviation, $\varepsilon_\Delta(\sigma)$ of the noise affecting the difference spectrum, $d(\sigma)$ under the assumptions of IASI correlated noise (Fig. 6(a) and IASI uncorrelated noise (Fig. 6(b)).

These computations have been done in simulation. First, we generated samples of random numbers with zero mean and standard deviation according to the IASI radiometric noise figures in Fig. 2. Second, these samples were passed through the same series of calculations as those that transform $r(\sigma)$ to $d(\sigma)$. In case we consider the effect of correlation, random numbers were generated according to the full IASI level 1C covariance matrix. The noise shown in Fig. 2 corresponds to the square root of the diagonal of the IASI covariance matrix.

Figure 6 also provides a comparison with the standard deviation obtained from a direct use of Eq. 11, with the appropriate band factor equal to $\sqrt{2/(0.68 - 0.65)} = 8.165$. It is seen that the comparison between simulation and Eq. 11 is perfect for the IASI uncorrelated noise. For the, real, case of IASI correlated noise, Eq. 11 slightly underestimates the standard deviation of the difference spectrum, $d(\sigma)$. Here and in the following the noise affecting $d(\sigma$ has been computed by considering correlated IASI noise at level 1C. Using the standard deviation expected for the difference spectrum (Fig. 6(a)) together with Eq. 16, we can easily compute the accuracy (that is the square root of var (q_{CO_2})) of the linear regression at each of the four channels at hand. The accuracy is shown in Tab. 1, which allows us to compare the results with the noise-free case.

Form Tab. 1 it is seen that the regression error increases of a factor 5 to 25, depending on the channel. However, we can optimally average the four different estimates, in order to improve the accuracy. To do so, it is important to realize that the d_j-channels may be correlated, so that we have to consider their proper covariance matrix in order to compute the optimal average.

Let $\mathbf{C}_d$ be the covariance matrix of the four channels. The size of $\mathbf{C}_d$ is 4×4 and it can be computed on simulations or directly by transforming the IASI covariance matrix from the

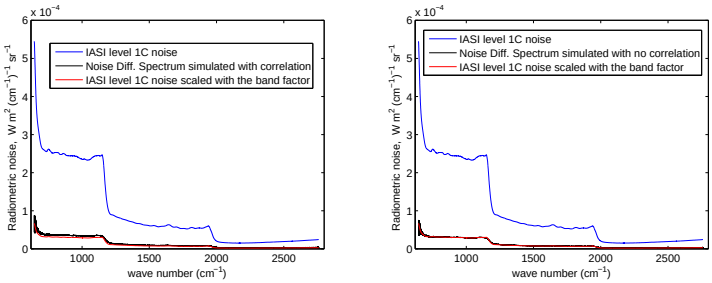

(a) with correlation (b) truly random

Fig. 6. Computation of the standard deviation of the noise affecting the difference spectrum in case of a partial interferogram extending from 0.65 to 0.68 cm. The computations have been made with IASI correlated noise (a) and IASI uncorrelated noise (b). A comparison is also provided with the standard deviation calculated with Eq. 11.

radiance space to the difference-radiance space. Whatever we do, this matrix can be computed in advance and stored for later applications, therefore it can be thought of as being a known parameter. Based on simulations, which made use of the IASI level 1C covariance matrix, we have that the couple (d_1, d_2) is slightly correlated with a correlation of 0.34, whereas the other combinations are truly un-correlated.

For a given IASI observation, let us suppose that we have computed through Eq. 15, the CO_2 amount, say q_j, corresponding to the four channels at σ_j, $j = 1, \ldots, 4$. Let us define $\mathbf{q} = (q_1, \ldots, q_4)^t$, where the super-script t denotes transpose operation. Let $\mathbf{A}_d$ be the 4×4 diagonal matrix, whose diagonal elements are the regression coefficients $(a_j/s_j)^2$. Then the covariance matrix, $\mathbf{C}_q$ of the vector $\mathbf{q}$ is the product $\mathbf{C}_q = \mathbf{A}_d \mathbf{C}_d \mathbf{A}_d^t$ and the optimal Least Squares estimation of, $\bar{q}_{CO_2}$ from the four estimates is given by

$$\bar{q}_{CO_2} = \frac{\mathbf{1}^t \mathbf{C}_q^{-1}}{\mathbf{1}^t \mathbf{C}_q^{-1} \mathbf{1}} \mathbf{q} \tag{17}$$

with the variance, $\mathrm{var}(\bar{q}_{CO_2})$ given by

$$\mathrm{var}(\bar{q}_{CO_2}) = \left(\mathbf{1}^t \mathbf{C}_q^{-1} \mathbf{1} \right)^{-1} \tag{18}$$

where $\mathbf{1} = (1, 1, 1, 1)^t$. Combining this way the four estimates, we have that the accuracy improves to the value of $\approx \pm 7$ ppmv.

One could say, why not to use more channels to get the accuracy close to the inherent limit of 1.5 ppmv? Well, the problem is that the more channels we use, the more the correlation among channels themselves increase. With high correlated channels, the optimal estimation does not improve so much in comparison to the channel with the best accuracy. Furthermore, another important point, which brings us to next section, is the sensitivity of the channels to the state vector. Since we have only access to a (possibly) best estimate of the atmospheric state corresponding to the given IASI observation, we need to make sure to select channels, which are loosely sensitive to the state vector, but CO_2.

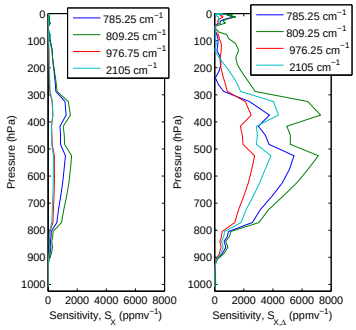

Fig. 7. For the four channels listed in the legend, panel a) shows the sensitivity of $r(\sigma)$ and panel b) that of $d(\sigma)$ to the CO_2 mixing ratio profile.

In this respect, the four channels, we are considering so long, show a very high sensitivity to CO_2. This is seen from Fig. 7, which compares $\mathbf{S}(\sigma)$ to $\mathbf{S}_\Delta(\sigma)$ for the case of a tropical model of the atmosphere. We see that the sensitivity to CO_2 improves of a factor 4-5 when passing from $r(\sigma)$ to $d(\sigma)$. Conversely, the sensitivity to the temperature profile (not shown for the sake of brevity) largely decreases when transforming from $r(\sigma)$ to $d(\sigma)$. The sensitivity analysis shows that the d_j-channels are sensitive to a large part of the troposphere, from to 900 to 100 hPa, which for the case of a tropical model of atmosphere encompasses all the troposphere above the Planetary Boundary Layer. Conversely, the d_j channels are almost insensitive to what happen in the boundary layer either for CO_2 or e.g. temperature, which is good because the lower troposphere is where we expect to have a larger uncertainty to the atmospheric state. In other words, also in case we implement the technique with a state vector which largely differs from the *truth* in the lower troposphere, we can still have valuable estimates for CO_2 provided the state vector is sufficiently accurate for the rest of the troposphere.

3.3 Application to IASI data for CO_2 estimation

The mechanics of the procedure to estimate the columnar amount of CO_2 can be summarized as follow,

- for a given IASI spectrum, choose the possibly best estimate of the state vector corresponding to the IASI overpass.
- With this state vector perform the radiative transfer calculations to yield synthetic IASI spectra (normally 4 are enough) corresponding to the different CO_2 columnar amounts in the range 300 to 450 ppmv.
- Transform the IASI spectra to difference spectra in order to estimate the regression coefficients of Eq. 15.
- Compute the observed d_j values from the IASI spectrum and input them to Eq. 15 to obtain the estimate at each channels.
- Finally, combine these estimates according to Eq. 17 and get the accuracy from Eq. 18

The best estimate of the state vector can be obtained in many modes e.g. colocated ECMWF analysis, radiosonde, inversion of IASI spectral radiances. For the work here shown, the state

vector is normally obtained from IASI spectral radiances themselves. As said in section 1 we use a retrieval methodology to which we refer as φ-IASI, whose mathematical aspects and validation has been largely documented (see e.g. Amato et al. (2002); Carissimo et al. (2005); Grieco et al. (2007); Masiello & Serio (2004); Masiello et al. (2009; 2011)).

To exemplify the procedure Fig. **??** shows the CO_2 columnar amount estimated for the 25 IASI soundings of the JAIVEx experiment. Figure **??**(a) also provides a comparison with the ECMWF analysis (Engelen et al., 2009). Although the two analysis are largely in agreement, we see that ECMWF tends to overestimate the CO_2 amount in comparison to the findings provided in this work. A comparison with aircraft in situ profiles (Grieco et al., 2011) shows that the analysis provided by our methodology is that correct. Finally, for illustrative purposes

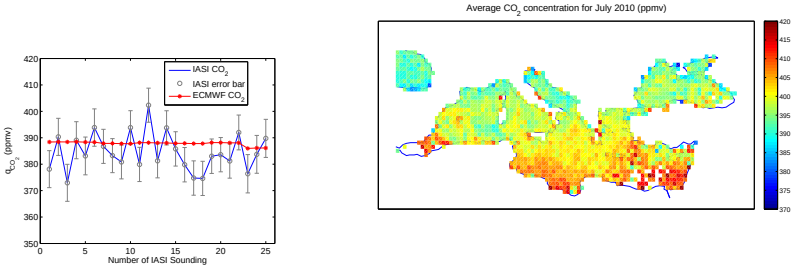

(a) JAIVEx case study

(b) Mediterranean case study

Fig. 8. (a)- CO_2 amount estimated from IASI (this work) and ECMWF analysis. (b)- IASI CO_2 for July 2010 over the Mediterranean area.

Fig. **??**(b) shows a monthly map of CO_2 computed for the Mediterranean area for the month of July 2010. This has been obtained by processing IASI spectra for July 2010 for sea surface. The spectra were checked for clear sky using the IASI stand alone cloud detection developed by Grieco et al. (2007); Masiello et al. (2002; 2003; 2004); Serio et al. (2000).

Figure **??**(b) clearly shows that the CO_2 amount is not a constant in the atmosphere. The North-to-South-East trend evidenced in the figure is consistent with the general circulation of the Mediterranean area, and is likely a consequence of the summer African anticyclone, which in July begins to extend its influence in the Mediterranean area. This possible effect is still under investigation with IASI data.

However, it is also important to stress that with a polar satellite such as METOP/1, the time-space data coverage is not uniform over the Mediterranean area, so that the spatial gradient has to be considered with some care and its assessment needs a suitable transport model. However, our finding is in agreement with similar maps derived by the Atmospheric Infrared Radiometer Sounder (AIRS) for the month of July (Chahine et al, 2008).

4. Application to CO

As for the case of CO_2, CO has well defined and known rotation transitions, which yield an absorption band, centered in between the atmospheric window at 4.67 μm (2142 cm^{-1}).

Because CO is a linear molecule, its strongest absorption features are regularly spaced and yield a periodic pattern, whose period is ≈ 4 cm^{-1} (see Fig. 9). This means that the

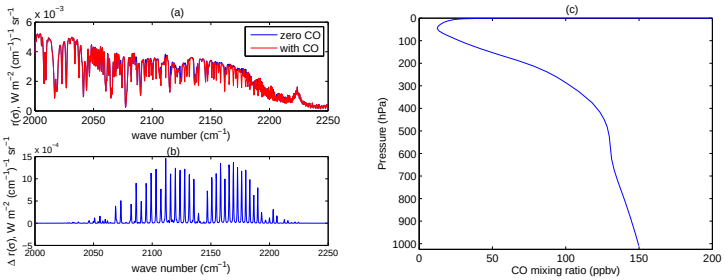

Fig. 9. The figure shows (a) two synthetic IASI spectra in the spectral region of CO absorption; one of the spectra has been calculated with zero load of CO. (b) The difference between the two evidences the sinusoidal appearance of the CO absorption features. Panel (c) shows the CO reference profile used for radiative transfer calculations.

interferogram has to show a characteristics beating due to CO at $x = 1/4$cm $= 0.25$ cm. We consider a partial interferogram extending from 0.21 to 0.31 cm for a width $\Delta x = 0.1$ cm. With the choice $\Delta x = 0.1$, the factor of noise reduction when we transform the radiance spectrum to the difference spectrum is approximately 4.45. In addition, since the CO band at 4.67 μm is completely covered by IASI band 3 (this extends from 2000 to 2760 cm^{-1}), the interferogram has been built up for band 3 alone. Finally, the reference CO profile is assumed from climatology and is shown in Fig. 9(c). The columnar amount is 109.12 ppbv (parts per billion per volume).

Figure 10 shows a detail of the interferogram in the optical path difference range 0.21 to 0.31 cm. The interferogram has been computed for a tropical model of atmosphere with the CO reference profile, shown in 9(c). A comparison with a case of zero CO load is also provided in the same figure. The corresponding difference spectra are shown in Fig. 10(b).

Unlike the case for CO_2, we have that in the range 0.21 to 0.31 cm, the interferogram gets much signal from the other emission atmospheric sources, which means that the CO signal may be masked from other emitting gases. Moreover, IASI band 3 is that of the three bands with lower signal-to-noise ratio.

However if we look at the difference spectrum, we see that around 2150 cm^{-1} there is a spectral region where the signal is almost determined by the CO signal alone. Once again this behaviour stresses that the difference spectrum can isolate emission feature of a given gas. Needless to say a search for d-channels which are mostly sensitive to CO shows that they are in the range 2150 to 2200 cm^{-1}. Three channels in this range, namely at 2191.25, 2193, 2195 cm^{-1}, provide estimates of the CO columnar amount, q_{CO} whose accuracy is in between 16 to 19 ppbv. Considering that the present average valus of atmospheric CO is around 109 ppbv, they allow an estimate with an accuracy within 15 to 20%. However, the channels are strongly correlated, therefore a methodology as that shown for CO_2 is not possible in this case. For this reason, we have focused on one single channel, that at 2195 cm^{-1}, which achieves the better retrieval performance for CO.

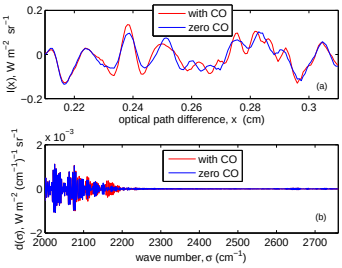

Fig. 10. (a) Inteferogram in the range 0.21 to 0.32 cm for a case of a tropical model of atmosphere; (b) the corresponding d-spectrum for the IASI band 3.

In a case of noise-free radiances the dependence of q_{CO} on $d(\sigma_1) \equiv d_1$, with $\sigma_1 = 2195$ cm^{-1} is parabolic on the full range, which spans from $q_{CO} = 0$ to $q_{CO} = 328$ ppbv. In terms of standardized quantities, the quadratic relation is

$$q_{CO} = a_1 D_1^2 + b_1 D_1 + c_1 \tag{19}$$

where the regression coefficients can be computed through simulation of synthetic radiances belonging to different values of CO columnar amount, q_{CO}. Doing so, we have found the result shown in Fig. 11, where we summarize the quadratic best fit for the two reference models of atmosphere: tropical and High Latitude Winter. As in the case of CO_2, we see that despite the large difference in the state vector, the quadratic fit is accurate for both models. Once we use the standardized difference-radiance, D_1 the regression coefficients do not depend on the atmospheric model. However, as in the case of CO_2 the standardization parameters, μ_1 and s_1 do depend on the state vector. In case of noise-free radiances the

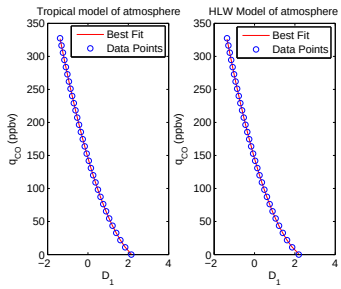

Fig. 11. Quadratic best fit of q_{CO} vs D_1 for (a) a tropical model of atmopshere and (b) a High Latitude Winter (HLW) model of atmopshere.

quadratic fit of Eq. 19 provides estimates for q_{CO} within ± 0.50 ppbv. In case of noisy radiances, the accuracy can be computed by the usual rule of variance propagation directly from Eq. 19, we have

$$\mathrm{var}(q_{CO}) = \left(2\frac{a_1}{s_1^2}d_1 + \frac{b_1}{s_1}\right)^2 \mathrm{var}(d_1) \tag{20}$$

For a tropical model of atmosphere the typical standard deviation of q_{CO} estimated by Eq. 19 is $\approx$ 16 ppbv (around 15% of its present climatological value). This figure increases to about

25 ppbv in a case of a High Latitude Winter air mass. These figures hold for one single IASI observation. The noise can be halved by considering an average over the 2× 2 pixel mask of the IASI FOV geometry.

As done for CO_2, the sensitivity of the CO d_1-channel to CO variations has been computed with the help of Eq. 12 and it is compared to that of the equivalent IASI spectrum-channel, $r(\sigma_1) \equiv r_1$ in Fig. 12. It is seen that the difference spectrum increase the sensitivity of factor two and more. The figure also allows us to get insight into understanding the atmospheric pressure-range at which the retrieval approach is sensitive. As for the case of CO_2, it is seen that the sensitivity extends to a broad range in between 900 to 100 hPa, therefore extending form the Planetary Boundary Layer to the upper troposphere. In contrast to the results of

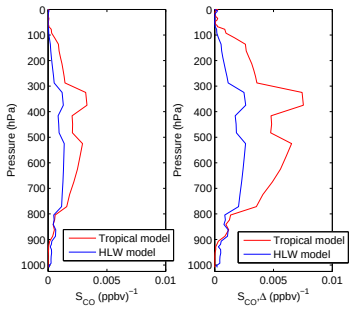

Fig. 12. Panel on the left: (a) Sensitivity of the IASI spectrum channel at 2195 cm^{-1} to CO variations for the case of two atmospheric models; (b) as in (a), but now the sensitivity is computed for the corresponding channel of the difference-spectrum.

Fig. 12, the sensitivity analysis shows that the d_1 channel at hand is poorly sensitive to other atmospheric parameters. This analysis is not shown here for the sake of brevity.

4.1 Application to IASI data

The mechanism of the procedure to estimate CO columnar amount from IASI observations is the same as that illustrated for CO_2 in section 3.3. During the JAIVEx experiment the CO profile was recorded by airborne in situ profiles (JAIVEx, 2007) recorded with the commercial gas instrument AL 5002 VUV Fast Fluorescence CO Analyser (produced by Aerolaser GmbH). The analyser employs the measurement of the fluorescence of CO when exposed to UV light at a wavelength of 150 nm, which is proportional to the concentration of CO. The measurements covered the lower-middle troposphere (1000 to 400 hPa) and extended to the upper part of the atmosphere based on climatology.

These CO profiles are shown in Fig. 13 and compared to the CO reference profile we have used to perform all the radiative transfer calculations needed to estimate the regression coefficients. It is seen from Fig.13 that the reference profile largely differs form those observed in the lower part of the troposphere. Below 400 hPa, the agreement is excellent, just because we use the same climatology as that used by the JAIVEx team. From Fig. 13 it is clearly seen that the CO profiles for 04 May 2007 are just a crude interpolation of that on 29 April 2007. Nevertheless, they have been included in the comparison with columnar CO retrieved

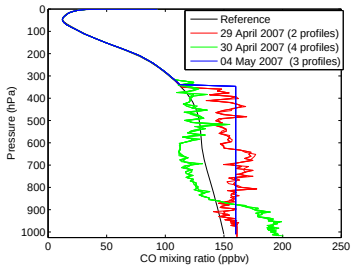

Fig. 13. CO profiles for two days of the JAIVEx experiemnt and comparison with the CO reference profile within the retrieval methodology to estimate the CO columnar amount.

from IASI for completeness and because these profiles constitute for that day the best in situ estimate of the CO profile.

Having said that, we see that the JAIVEx experiment provides a case study in which the CO reference profile is different from the supposedly correct CO profile corresponding to the JAIVEx campaign (see Fig.13). Thus, we have a case study in which the shape of the profile, and not only the CO integrated amount, differs form that of the reference profile. This situation allows us to check the sensitivity of the methodology to the shape of the CO profile.

The results of our methodology applied to the 25 IASI soundings during the JAIVEx experiment are shown in Fig. 14(a) along with the estimation of the columnar amount from in situ measurements. This last estimate has been obtained by integrating the CO mixing ratio profile (see Fig.13(a)) for each day of the JAIVEx experiment. For each day, the corresponding in situ estimates (2 for 29 April 2007, 4 for 30 April 2007, and 3 for 04 May 2007) have been averaged and these three average values are shown as flat lines in Fig. 14(a). The comparison

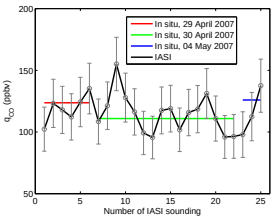

(a) JAIVEx case study

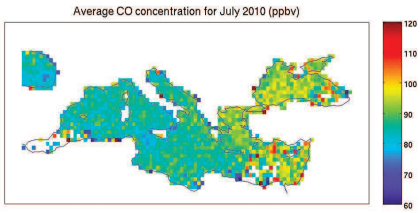

(b) Mediterranean case study

Fig. 14. (a)- CO integrated amount estimated from IASI (this work) and in situ observations. (b)- IASI CO for July 2010 over the Mediterranean area.

provided in Fig. 14 shows that IASI agrees with the in situ observations in evidencing a slight

decrease of the CO load for the target area on 30 April 2007 in comparison to those over passed by IASI on 29 April and 04 May, respectively. This is also evidenced if we compare the average values for the day 29 April 2007 and 30 April 2007. For 29 April 2007 we have a mean value of (119.6 ± 7.0) ppbv for IASI against a value of 123.7 ppbv estimated from in situ observations. For the day 30 April 2007, both IASI and in situ observations show a lower value for the CO load, IASI (114.2 ± 4.2) ppbv, in situ 111.0 ppbv.

Finally, as done for CO_2, for illustrative purposes Fig. 14(b) shows a monthly map of CO computed over the Mediterranean area for the month of July 2010.

5. Application to CH_4

Unlike CO and CO_2, methane is not a linear molecule, therefore we have no particular hint from its structure about which interval of the interferogram is most sensitive to the variation of this gas. However, methane together with water vapour, is the main absorber within IASI band 2, which means that if we consider the interferogram of IASI band 2 alone, we should be able to isolate a suitable portion of the interferogram signal, which is mostly dominated by CH_4. By trial and error this interval has been identified in the segment 1.34-1.352 cm, for a bandwidth of 0.0120 cm. With this reduced bandwidth, according to Eq. 11, we have a noise reduction within the difference spectrum of 12.90. Actually, because of the effect of IASI noise correlation, the reduction factor is even higher. If we consider that for IASI band 2 we have the better signal-to-noise ratio, we have that methane is the gas, which we can retrieve with the highest stability and accuracy. In particular the channels in the spectral segment 1210 to 1220 cm^{-1} exhibit the poorest sensitivity to the state vector, but methane.

A good channel is that at $\sigma = 1210.75$ cm^{-1}. The regression relation between the channel and the methane columnar amount is a polynomial of third order. The regression error is 0.01 ppmv in case of noise-free radiances and $\approx$ 0.1 ppmv in case of noisy radiances. The regression relation is invariant with the state vector as it is shown in Fig. 15. The CH_4 reference profile we use for the radiative transfer calculation is that shown in Fig. 15(d), which gives a columnar amount for methane of 1.65 ppmv. The sensitivity, $S_{CH_4,\Delta}(\sigma)$ of the d-spectrum (channel at $\sigma = 1210.75$ cm^{-1}) to methane is shown in 15(c) for the tropical and High Latitude Winter models of atmosphere, whose main atmospheric parameters have been shown in Fig. 4

5.1 Application to IASI data

The mechanism of the procedure to estimate CH_4 columnar amount from IASI observations is the same as that illustrated for CO_2 in section 3.3. The procedure for methane has been applied to the 25 IASI spectra and the results are shown in Fig. 16(a). We see that the columnar amount is very stable and varies in between 1.60-1.90 ppmv with an average of (1.70 ± 0.02) ppmv. We remember that this data were acquired in 2007. Today the average global value of methane is credited of a value equal to 1.74 ppmv (Blasing, 2011). During the JAIVEx experiment there were no in situ observations of methane. However, we can perform a consistency check about the observed and computed variability. According to our procedure, the accuracy of the estimates is $\approx$ 0.094 ppmv. Because the JAIVEx case study consider a limited target area, we have to expect a very low variability as far as the columnar amount of CH_4 is considered. This means that the variability we see in Fig. 16(a) has to be largely due

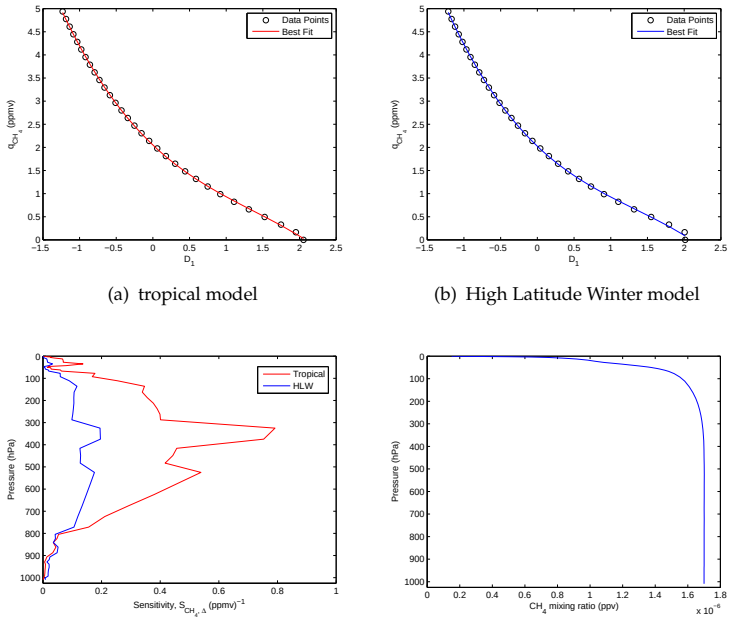

(a) tropical model

(b) High Latitude Winter model

(c) Sensitivity to CH_4

(d) CH_4 reference profile

Fig. 15. The polynomial fit at 1210.75 cm^{-1} exemplified for two models of atmosphere, (a) and (b); the sensitivity to methane (c); the reference methane mixing ratio profile (d).

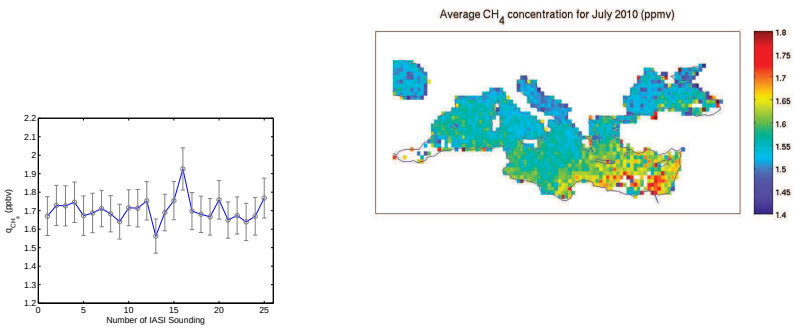

(a) JAIVEx case study

(b) Mediterranean case study

Fig. 16. (a)- CH_4 integrated amount estimated from IASI. (b)- IASI CH_4 for July 2010 over the Mediterranean area.

to random fluctuations, therefore the standard deviation of the 25 IASI estimates has to be consistent with the computed accuracy of 0.094 ppmv. In fact, this standard deviation gives

the value 0.0945 ppmv.

Finally, as done for CO_2 and CO, for illustrative purposes Fig. 16(b) shows a monthly map of CH_4 computed over the Mediterranean area for the month of July 2010. Also for CH_4, the map clearly shows a gradient in the North-to-South direction, which is consistent with the general circulation of the Mediterranean area.

6. Application to N_2O

As for the methane, N_2O is not a linear molecule, therefore partial interferograms, which are capable of enhancing the variations of this gas with respect to those of other dominant atmospheric parameters, have to be be judiciously found by careful inspections of synthetic interferogram signals generated as a function of N_2O columnar amount, q_{N_2O}. Using this strategy we have found that the partial interferogram in the range 1.06-1.08 cm for a width of 0.02 cm is largely sensitive to N_2O. With this reduced bandwidth, according to Eq. 11, we have a noise reduction within the difference spectrum of 10. Actually, because of the effect of IASI noise correlation, the reduction factor is even higher. However, we have to consider that N_2O absorption insists within the IASI band 3, which is that with the worse signal-to-noise ratio. With this in mind we have that accuracy with which we can estimate q_{N_2O} is of the order of 10% at the level of single channels. In addition, *good* channels tend to be strongly correlated, therefore there is no advantage in trying to combine them to improve the final accuracy.

The regression relation which fit to the data with an error of less than 3 ppbv is a polynomial of fourth order. The polynomial is independent of the atmospheric sate vector as it is shown in Fig. 17 which exemplifies the polynomial regression for the case of the d-channel at 2165.50 cm^{-1}.

The N_2O reference profile we use for the radiative transfer calculation is that shown in Fig. 17(d), which gives a columnar amount for N_2O of 306.5 ppbv. The sensitivity, $S_{N_2O,\Delta}(\sigma)$ of the d-spectrum (channel at $\sigma = 2204.5$ cm^{-1}) to N_2O is shown in 17(c) for the tropical and High Latitude Winter models of atmosphere, whose main atmospheric parameters have been shown in Fig. 4

6.1 Application to IASI data

The philosophy and mechanism of the procedure to estimate N_2O columnar amount from IASI observations is the same as that illustrated for CO_2 in section 3.3. For N_2O, the procedure has been applied to the 25 IASI spectra and the results are shown in Fig. 18(a). We see that the columnar amount varies in between 250-450 ppbv with a peak-to-peak variability of about 200 ppbv, although the standard deviation of the data ($\approx$ 41 ppbv) is consistent with the accuracy of each single observation, which is around 40 ppbv. The average value over the 25 soundings is 303 ppbv. This is a bit lower than the today average global mean value ($\approx$ 323 ppbv (Blasing, 2011)) estimated based on in situ observations at ground level stations. However, N_2O may be characterized by large anomaly from its mean global value even on monthly time scales (Blasing, 2011; Lubrano et al., 2004; Ricaud et al., 2009). However, if we consider the monthly map of N_2O computed over the Mediterranean area for the month of July 2010 (see Fig. 18(b)), we see that the average concentration comes closer to the monthly values normally observed with in situ observation at ground level stations.

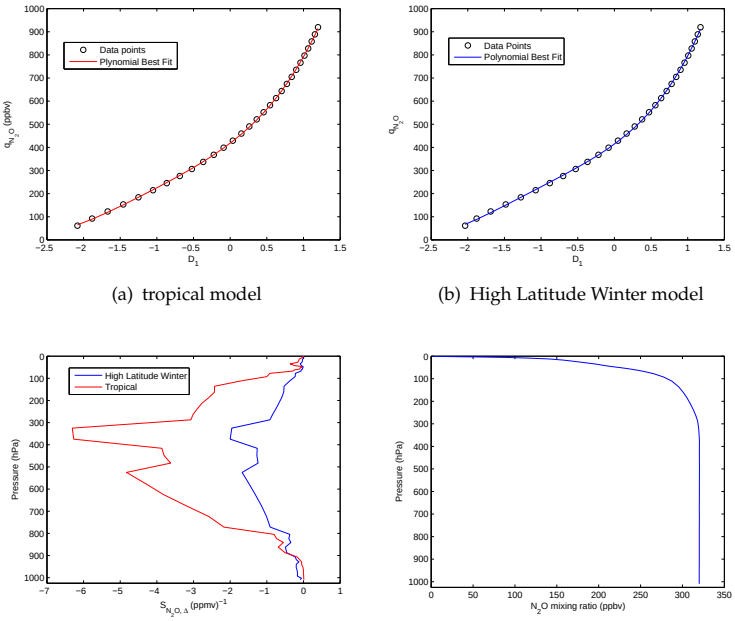

(a) tropical model

(b) High Latitude Winter model

(c) Sensitivity to N_2O

(d) N_2O reference profile

Fig. 17. The polynomial fit at 2165.50 cm^{-1} exemplified for two model of atmosphere, (a) and (b); the sensitivity to N_2O (c); the reference N_2O mixing ratio profile (d).

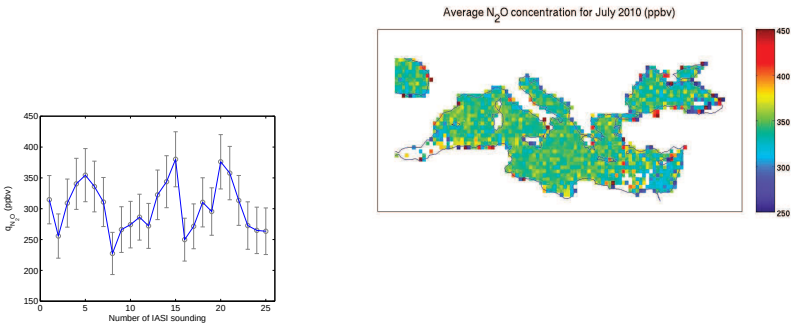

(a) JAIVEx case study

(b) Mediterranean case study

Fig. 18. (a)- N_2O integrated amount estimated from IASI. (b)- IASI N_2O for July 2010 over the Mediterranean area.

7. Conclusion

We have described and presented the basic aspects of Fourier Spectroscopy with Partially Scanned Interferogram and exemplified its application to the retrieval of minor and trace gases in the atmosphere. Observations from the IASI instrument have been considered and the technique has been applied to estimate the columnar amount of CO_2, CO, CH_4 and N_2O.

The retrieval algorithms we have implemented rely on simple polynomials regression relations, whose coefficients, once properly standardized, are independent of the atmospheric state. However, the technique still needs the standardization parameters, which may depend on the state vector. Thus, the procedure still relies on the availability of a suitable a-priori best estimate of the atmospheric state vector. We have shown that this best estimate can be confidently obtained by previously inverting IASI radiances for skin temperature, and temperature, water vapour and ozone profiles. The accuracy of this *best estimate* can be by far lower than that expected from IASI radiances themselves. We have shown that uncertainty about the temperature profile of the order of $\pm$2K along the profile are easily tolerated. For water vapour we can easily tolerate with uncertainties of more than $\pm$20%, along the profile. Furthermore, the technique is largely insensitive to the surface emission.

FTS*PSI is a truly novel methodology as far as its applications to high spectral resolution infrared observations is concerned. The tools we have presented in this work have not been particularly optimized. Nevertheless, their applications to atmospheric gases yielded impressive results for accuracy and quality, which are unprecedented if compared to those normally obtained with the usual machinery of inverting spectral radiances. We think that the capability of the methodology has been only scratched at the surface, and we hope this study can soon attract attention and stimulate new research studies, which can hopefully exploit the many facets of the tool.

Acknowledgements IASI has been developed and built under the responsibility of the Centre National d'Etudes Spatiales (CNES, France). It is flown onboard the Metop satellites as part of the EUMETSAT Polar System. The IASI L1 data are received through the EUMETCast near real time data distribution service. We thank Dr Stuart Newman (Met Office) for providing the JAIVEx data. The JAIVEx project has been partially funded under EUMETSAT contract Eum/CO/06/1596/PS. The FAAM BAe 146 is jointly funded by the Met Office and the Natural Environment Research Council. The US JAIVEx team was sponsored by the National Polar-orbiting Operational Environmental Satellite System (NPOESS) Integrated Program Office (IPO) and NASA.

8. References

Amato, U.; De Canditiis, D.; Serio, C. (1998). Effect of apodization on the retrieval of geophysical parameters from Fourier-Transform Spectrometers. *Appl. Opt.*, 37, 6537-6543.

Amato, U.; Masiello, G.; Serio, C.; Viggiano, M. (2002). The σ-IASI code for the calculation of infrared atmospheric radiance and its derivatives. *Environ. Model. Software*, 17, 651-667.

Bell, R.J. (1972). *Introductoiy Fuorier Transform Spectroscopy*, Acad.Press, New York.

Blasing, T.J. (2011), Recent Greenhouse Gas Concentrations, DOI: 10.3334/CDIAC/atg.032

Boynard, A.; Clerbaux, C.; Coheur, P.-F.; Hurtmans, D.; Turquety, S.; George, M.; Hadji-Lazaro, J.; Keim, C.; Mayer-Arnek, J. (2009). Measurements of total and tropospheric ozone from the IASI instrument: comparison with satellite and ozonesonde observations, *Atmos. Chem. Phys.*, 9, 6255-6271.

Carissimo, A.; De Feis, I.; Serio, C. (2005). The physical retrieval methodology for IASI: the δ-IASI code. *Environ. Model. Software*, 20, 1111–1126.

Chevalier, F. (2001) *Sampled Database of 60 Levels Atmospheric Profiles from the ECMWF Analysis*; Technical Report; ECMWF EUMETSAT SAF programme Research Report 4; ECMWF: Shinfield Park, Reading, UK.

Chahine M.T.; Barnet, C.; Olsen, E.T.; Chen, L.; Maddy, E. (2005). On the determination of atmospheric minor gases by the method of vanishing partial derivatives with application to CO_2, *Geophys. Res. Lett.*, 32, L22803, doi:10.1029/2005GL024165.

Chahine, M. T.; Chen, L.; Dimotakis, P.; Jiang, X.; Li, Q.; Olsen, E. T.; Pagano, T.; Randerson, J.; Yung Y. L. (2008). Satellite remote sounding of mid-tropospheric CO_2, *Geophys. Res. Lett.*, 35, L17807, doi:10.1029/2008GL035022.

Clarisse, L.; Coheur, P. F.; Prata, A. J.; Hurtmans, D.; Razavi, A.; Phulpin, T.; Hadji- Lazaro, J.; Clerbaux, C. (2008). Tracking and quantifying volcanic SO2 with IASI, the September 2007 eruption at Jebel at Tair, *Atm. Chem. Phys.*, 8, 7723-7734.

Clarisse L., Clerbaux, C.; Dentener, F.; Hurtmans, D.; Coheur, P.-F. (2009). Global ammonia distribution derived from infrared satellite observations, *Nature Geosci.*, 2, 479- 483, doi:10.1038/ngeo551

Clerbaux C.; A. Boynard, A.; Clarisse, L.; M. George, M.; Hadji-Lazaro, J.; Herbin, H.; Hurtmans, D.; Pommier, M.; Razavi, A.; Turquety, S.; Wespes, C.; Coheur, P.-F. (2009). Monitoring of atmospheric composition using the thermal infrared IASI/Metop sounder, *Atmos. Chem. Phys.*, 9, 6041-6054.

Crevoisier, C.; Chédin, A.; Matsueda, H.; Machida, T.; Armante, R.; Scott, N. A. (2009). First year of upper tropospheric integrated content of CO_2 from IASI hyperspectral infrared observations. *Atmos. Chem. Phys.*, 9, 4797-4810, doi:10.5194/acp-9-4797-2009.

Engelen, R.J.; Serrar, S.; Chevallier, F. (2009). Four dimensional data assimilation of Atmospheric CO_2 using AIRS observations. *J. Geophys. Res.*, 114, D03303, doi:10.1029/2008JD010739.

Gardiner, T.; Mead, M. I.; Garcelon, S.; Robinson, R.; Swann, N.; Hansford, G. M.; Woods, P. T.; Jones, R. L. (2010). A lightweight near-infrared spectrometer for the detection of trace atmospheric species. *Rev. Sci. Instrum.* 81, 083102; doi:10.1063/1.3455827 (11 pages).

Goldstein, H. W.; Grenda, R. N.; Bortner, M. H.; Dick, R. (1978). CIMATS: a correlation interferometer for the measurements of atmospheric trace species. *Proceedings of the 4th Joint Conference on Sensing of Environmental Pollutants*. American Chemical Society, 586Ű589.

Grieco, G.; Masiello, G.; Matricardi, M.; Serio, C.; Summa, D.; Cuomo, V. (2007). Demonstration and validation of the φ-IASI inversion scheme with NAST-I data, *Q. J. R. Meteorol. Soc.*, 133, 217-232.

Grieco, G.; Masiello, G.; Serio, C. (2010). Interferometric vs Spectral IASI Radiances: Effective Data-Reduction Approaches for the Satellite Sounding of Atmospheric Thermodynamical Parameters. *Remote Sens.* 2, 2323-2346.

Grieco, G.; Masiello, G.; Serio, C.; Jones, R.L.; Mead, M.I. (2011). Infrared Atmospheric Sounding Interferometer correlation interferometry for the retrieval of atmospheric gases: the case of H_2O and CO_2. *Appl. Opt.* 50, 4516-4528. doi:10.1364/AO.50.004516

FAAM, "Joint Airborne IASI Validation Experiment (JAIVEX)" http://badc.nerc.ac.uk/data/jaivex/

Kyle, T.G. (1977). Temperature soundings with partially scanned interferograms. *Appl. Opt.*, 16/2, 326-332.

Lubrano, A.M.; Masiello, G.; Matricradi, M.; Serio, C.; Cuomo, V. (2004). Retrieving N_2O from nadir-viewing infrared spectrometers. *Tellus B*, 56(3), 249 - 261.

Masiello, G.; Matricardi, M.; Rizzi, R.; Serio, C. (2002). Homomorphism between Cloudy and Clear Spectral Radiance in the 800-900-cm^{-1} Atmospheric Window Region. *Appl. Opt.* 41, 965-973. doi:10.1364/AO.41.000965

Masiello, G.; Serio, C; Shimoda, H. (2003). Qualifying IMG tropical spectra for clear sky. *Journal of Quantitative Spectroscopy and Radiative Transfer.* 77/2, 131-148. doi:10.1016/S0022-4073(02)00083-3

Masiello, G.; Serio, C.; Cuomo, V. (2004). Exploiting Quartz Spectral Signature for the Detection of Cloud-Affected Satellite Infrared Observations over African Desert Areas. *Appl. Opt.* 43, 2305-2315. doi:10.1364/AO.43.002305

G. Masiello, G.;& Serio, C. (2004). Dimensionality-reduction approach to the thermal radiative transfer equation inverse problem. *Geophys. Res. Lett.*, 31, L11105, doi:10.1029/2004GL019845.

Masiello, G.; Serio, C.; Carissimo, A.; Grieco, G. (2009). Application of ϕ-IASI to IASI: retrieval products evaluation and radiative transfer consistency. *Atmos. Chem. Phys.*, 9, 8771-8783.

Masiello, G.; Matricardi, M.; Serio, C. (2011). The use of IASI data to identify systematic errors in the ECMWF forecasts of temperature in the upper stratosphere. *Atmos. Chem. Phys.*, 11, 1009-1021, doi:10.5194/acp-11-1009-2011.

K. Masuda, K.; Takashima, T.; Takayama, Y. (1988). Emissivity of pure and sea waters for the model sea surface in the infrared window regions, *Remote Sens. Environ.*, 24, 313-329.

McMillan W. W., C. Barnet, L. Strow, M. T. Chahine, M. L. McCourt, J. X. Warner, P. C. Novelli, S. Korontzi, E. S. Maddy, S. Datta (2005), "Daily global maps of carbon monoxide from NASA's Atmospheric Infrared Sounder", Geophys. Res. Lett., 32, L11801, doi:10.1029/2004GL021821.

Pichett, H.M.; & Strauss, H.L. (1972). Signal-to-Noise ratio in Fourier spectrometry, *Analytical Chemistry*, 44(2), 265-270.

Ricaud, P.; Attié, J.-L.; Teyssédre, H.; El Amraoui, L.; Peuch, V.-H.; Matricardi, M.; Schluessel, P. (2009). Equatorial total column of nitrous oxide as measured by IASI on MetOp-A: implications for transport processes, *Atmos. Chem. Phys.*, 9, 3947-3956, doi:10.5194/acp-9-3947-2009.

Robinson, E.A.;& Silvia, M.T. (1981). *Digital Foundation of Time Series Analysis: Wave-Equation Space-Time Processing*, Vol. 2 Holden-Day, San Francisco.

Serio, C.; Lubrano, A.M.; Romano, F.; Shimoda, H. (2000). Cloud Detection Over Sea Surface by use of Autocorrelation Functions of Upwelling Infrared Spectra in the 800Ű900-cm^{-1} Window Region. *Appl. Opt.* 39, 3565-3572, doi:10.1364/AO.39.003565

Smith, W.L.; Howell, H.B.; Woolf, H.M. (1979). The use of interferometric radiance measurements for the sounding the atmosphere. *Appl. Opt.*, 36, 566-575.